

Renormalization of the Optical Response of Semiconductors by Electron-Phonon Interaction

MANUEL CARDONA

Max-Planck-Institut für Festkörperforschung,
Heisenbergstr. 1, 70569 Stuttgart, Germany
cardona@kmr.mpi-stuttgart.mpg.de

August 7, 2001

PACS: 78.20.Ci, 78.20.Nv, 65.70.+y, 63.20.Kr, 62.20.Dc

In the past five years enormous progress has been made in the *ab initio* calculations of the optical response of electrons in semiconductors. The calculations include the Coulomb interaction between the excited electron and the hole left behind, as well as local field effects. However, they are performed under the assumption that the atoms occupy fixed equilibrium positions and do not include effects of the interaction of the lattice vibrations with the electronic states (electron-phonon interaction). This interaction shifts and broadens the energies at which structure in the optical spectra is observed, the corresponding shifts being of the order of the accuracy claimed for the *ab initio* calculations. These shifts and broadenings can be calculated with various degrees of reliability using a number of semiempirical and *ab initio* techniques, but no full calculations of the optical spectra including electron-phonon interaction are available to date.

This article discusses experimental and theoretical aspects of the renormalization of optical response functions by electron-phonon interaction, including both temperature and isotopic mass effects. Some of the theoretical techniques used can also be applied to analyze the renormalization of other response functions, such as the phonon spectral functions, the lattice parameters, and the elastic constants.

1 Introduction

The temperature dependence of macroscopic properties of crystals (i.e., specific heat [1–3], thermal expansion [4], thermal conductivity [5,6], elastic constants [7]) played an important role in the early development of the quantum theory of solids [1–4]. More recently, the temperature dependence of microscopic properties, involving spectroscopic elementary excitations such as those responsible for optical absorption and reflection [8,9] and phonons [10] have been discussed both experimentally and theoretically. The theoretical treatments have ranged from semiempirical ones [1–4,8,9] to state-of-the-art *ab initio* calculations [10,11].

During the past five years considerable progress has been made in calculating *ab initio* the linear response functions, i.e., the complex dielectric functions of semiconductors and insulators [12–14]. These calculations, which include the Coulomb interaction between the excited electron and the hole left behind in the valence band (the so-called excitonic interaction) and local-field effects, represent an enormous improvement over the early semiempirical calculations [15,16]. They nevertheless implicitly assume that the constituent atoms occupy fixed positions and thus neglect the effects of the lattice vibrations on the electronic structure, i.e., the electron-phonon interaction. Such effects have been calculated for selected transition energies (at so-called interband critical points, CP) [8,9,11], but calculations of the full spectrum of electronic interband transitions including electron phonon-interaction effects are yet to be performed.

Considerable effort has been devoted to experimental studies of the effect of external perturbations on the dielectric function of solids. Among these perturbations we mention static strain [17,18], electric fields [19], magnetic fields [20], and sublattice displacements corresponding to optical phonons with $\mathbf{q} = 0$ [21]. The latter determine the frequency dependence of Raman spectra. The contribution of a crystal surface to the linear optical response has also been profusely studied. Several articles in these proceedings deal with this subject, both experimentally and theoretically, the theoretical work being not as advanced as that mentioned above for the bulk. In any case it does not include *ab initio* the effects of the electron-phonon interaction either. Nor do the rather simplified calculations which have been performed for the effect of strain [17,22,23] or electric fields [24] on the dielectric function.

The effect of “temperature” on optical spectra of crystals results from the interaction of the electronic states with the vibrations of the lattice (electron-phonon interaction), an effect which does not vanish even for $T = 0$. According to quantum mechanics, the vibrational amplitude does not vanish at $T = 0$: the so-called zero-point vibrational amplitude remains and is responsible for energy renormalizations up to 100 meV, of the order of the accuracy claimed for state-of-the-art *ab initio* calculations of critical point energies in such spectra [12–14,25].

Zero-point vibrational amplitudes should vanish, in a *gedankenexperiment*, when the ionic masses of a crystal become infinitely large. In the past 12 years, many crystals with variable isotopic compositions have become available. It has therefore become possible to measure the dielectric functions $\epsilon(\omega)$ of crystals with different isotopic masses, to extrapolate them to infinite values of M and thus obtain experimentally the bare values of transition energies [25–28]. It may sound paradoxical that one can obtain bare, i.e., unrenormalized, parameters from experiment since only renormalized parameters, including all self-energy corrections such as those due to electron-phonon interaction, are observable. However, as pointed out by Allen [29], the procedure to obtain unrenormalized parameters just described is only an approximate one. It requires assumptions which lead to a simple dependence of the zero-point renormalization on isotopic mass and temperature, in particular the truncation of the electron-phonon perturbation theory series after the second-order terms.

In this paper we describe the three contributions which lead to the temperature dependence of optical transition energies (including zero-point effects) in crystals, up to second-order perturbation theory. They are:

- i*) The effect of the first-order electron-phonon interaction Hamiltonian to second-order in perturbation theory. These are the so-called Fan terms [8].
- ii*) The effect of second-order electron-phonon interaction in first-order perturbation theory [30]. These are Debye-Waller terms, sometimes also referred to as Yu-Brooks terms [9].

iii) The effect of thermal expansion, including zero-point renormalization of lattice parameters, coupled with the dependence of the transition energies on such parameters [8].

We shall discuss simple algebraic expressions which have been used to fit the measured dependences of transition energies (also called gaps or critical points, CP's) on temperature, together with the related effects of isotopic mass on CP's. The effect mentioned above under *(i)* is described in terms of complex self-energies $\Sigma = \Sigma_r + i \Sigma_i$, which encompass not only energy shifts (Σ_r) but also broadenings of the optical features (Lorentzian-HWHM = $-\Sigma_i$). The effects *(ii)* and *(iii)* correspond to real energy shifts of CP's or energy gaps. Emphasis is placed in this article on a method of obtaining zero-point renormalization through extrapolation to zero temperature of the linear part of the shift of CP energies with temperature usually found at high temperatures. Extension of these phonon renormalization to other more macroscopic physical properties, such as lattice parameters (needed also for the evaluation of the *(iii)* terms), elastic constants, and phonon frequencies, is also discussed.

2 Renormalization of Electronic States through Electron-Phonon Interaction

The renormalization of excitation energies by lattice vibrations (or other perturbing agents such as disorder) is represented, in the many-body theory of solids, by a frequency (= energy for $\hbar = 1$, a value of \hbar which will be assumed implicitly throughout this paper) and wavevector dependent self-energy $\Sigma(\omega, \mathbf{k}) = \Sigma_r(\omega, \mathbf{k}) + i \Sigma_i(\omega, \mathbf{k})$. While the bare excitation energy $\omega(\mathbf{k})$ is real, i.e., the excited “particles” with a well-defined real wavevector \mathbf{k} have an infinite lifetime, the imaginary part of the self-energy adds an imaginary component to the excitation energy and the excited “particle” acquires a finite lifetime τ for a real value of \mathbf{k} , i.e., it becomes a “quasiparticle”. This lifetime of the corresponding electron-hole excitation is given by the uncertainty-principle-like expression:

$$\tau = (-2 \Sigma_i)^{-1} , \quad (1)$$

the minus sign resulting from the convention chosen for the sign of Σ_i ($\Sigma_i \leq 0$). We are concerned here with frequency renormalizations induced by phonons of frequency $\Omega(\mathbf{q})$ and harmonic vibrational amplitude $u(\Omega, \mathbf{q})$. Because the time average of u is zero (in the harmonic approximation, perturbation terms of first-order in $u(\Omega, \mathbf{q})$ vanish in $\Sigma(\omega, \mathbf{k})$). Such terms are responsible for a broad, incoherent (i.e., that does not correspond to a single value of \mathbf{k}) background which will not concern us here, except in so far as it has been incorrectly interpreted sometimes to generate a finite value of $\Sigma_i(\omega, \mathbf{k})$ [31].

2.1 Thermal expansion effects

As already mentioned, the calculation of $\Sigma(\omega, \mathbf{k})$ is broken up into two parts. One of them involves a perturbation calculation keeping the solid at constant volume (i.e., keeping the shape of the primitive cell and the Brillouin zone, BZ, constant). However, the experiments are not performed at constant volume, but at constant pressure. Hence, we must add to the perturbation results just mentioned the effect of thermal expansion at constant pressure (usually atmospheric, for practical purposes zero):

$$\Delta\omega_0 = \left(\frac{\Delta V(T)}{V_0} \right)_p \cdot a = \left(\frac{\Delta V(T)}{V(0)} \right)_p \cdot B_0 \cdot \left(\frac{\partial\omega_0}{\partial p} \right)_T \quad (2)$$

where $\Delta V(T) = V(T) - V_0$ is the change in volume induced by the temperature T and a is the change in transition energy ω_0 induced by the change in volume, the so-called hydrostatic deformation potential of the CP under consideration. Usually one measures the dependence of ω_0 on pressure, in which case $\Delta\omega_0$ must be obtained from the r.h.s. of (1) using the bulk modulus B_0 and the pressure dependence of ω_0 represented by $(\partial\omega_0/\partial p)$.

The thermal expansion $(\Delta V(T)/V_0)_p$ results from *anharmonic* terms in the expansion of the crystal energy vs. atomic displacement, whereby only odd terms in this expansion contribute (or combinations of odd and even terms, with an odd number of odd terms): The even terms average to zero and do not change the equilibrium position of the atoms. We shall keep for our discussion only the lowest (third) order anharmonic terms which lead to a linear dependence of $\Delta V(T)$ on T at high temperature, i.e., to a T -independent thermal expansion coefficient in this T range. These terms are conveniently represented by the *mode Grüneisen parameter* $\gamma_n(\mathbf{q})$ defined as:

$$\gamma_n(\mathbf{q}) = - \frac{V_0}{\Omega_n(\mathbf{q})} \left(\frac{\partial\Omega_n(\mathbf{q})}{\partial V} \right)_{V_0} \quad (3)$$

where \mathbf{q} is the wavevector of a generic phonon and n its branch index. Using thermodynamic relations, and minimizing the free energy at “zero pressure” and temperature T , one finds [32,33]:

$$V(T) = V_0 + \frac{1}{2B_0} \sum_{n,\mathbf{q}} \Omega_n(\mathbf{q}) \gamma_n(\mathbf{q}) (2n_B + 1) \quad (4)$$

where n_B is the Bose-Einstein statistical factor:

$$n_B(\Omega, T) = [e^\xi - 1]^{-1} ; \xi = \frac{\Omega}{T} , \quad (5)$$

with T in the same units as Ω . Note that Eq. (4) allows us to calculate not only the temperature dependence of the crystal volume, but also the zero temperature renormalization, by setting $n_B = 0$ [32–35]. In elemental crystals this zero-point renormalization is proportional to $M^{-\frac{1}{2}}$, where M is the average isotopic mass.

In order to evaluate the thermal expansion contribution to $\Delta\omega_o$ (including zero-point effects) with Eq. (2) one can use either experimental values of $(\Delta V(T)/V_0)$ [36,37] or those calculated with Eq. (4). The former are obtained rather accurately by means of X-ray diffraction. For the latter procedure one can use either experimental values of $\gamma_n(\mathbf{q})$ [38] or values calculated using *ab initio* band structure techniques [32,33]. One should mention, at this point, that the $\gamma_n(\mathbf{q})$, which according to (4) should have an average value of about +1, is negative ($\simeq -1$) for the TA phonons at the edge of the BZ of most germanium and zincblende-type semiconductors (exceptions: diamond [38] and, curiously enough, CuI [38,39]). When these negative values are entered into Eq. (2) they lead to anomalous negative expansion coefficients at temperatures close to the frequencies of the corresponding phonons. At much lower temperatures, the expansion coefficients become usually (but not always [33]) positive again. This results in a very flat dependence of $V(T)$ vs. T for T below the TA-phonon frequencies [37,40]. The oscillations due to the sign reversals of $\gamma_n(\mathbf{q})$ are easy to see in the expansion coefficient vs. T which corresponds to the *derivative* of $V(T)$ vs. T . They are hardly noticeable in $\Delta V(T)$ except that

the behavior of $\Delta V(T)$ vs. T is very flat at low temperatures. It is therefore very difficult to see the corresponding effects in the contribution to $\Delta\omega_0$ given in Eq. (2), a fact which, however, makes easier the analysis of data on the temperature dependence of electronic CP energies.

2.2 Electron-phonon interaction

The direct electron-phonon interaction terms, defined for a temperature independent volume, are responsible for the “explicit effect” of temperature on the electron energies. The term “implicit effects” is applied to the thermal expansion contribution discussed in 2.1. The two terms displayed as Feynman diagrams in Fig. 1 contribute to the phonon renormalization of one-electron states to the same order in perturbation theory as that used in 2.1. Electronic excitations involve an excited electron in the conduction band and a hole left behind in the valence band. It is easy to show that the renormalization can be obtained as the difference of two sets of diagrams of the type in Fig. 1, the electron diagram minus the hole diagram, provided one neglects vertex terms which connect electron and hole lines [41]. Diagram (i), representing the first-order perturbation Hamiltonian taken to second order in perturbation theory, leads to a complex self-energy whose imaginary part Σ_i represents the Lorentzian width (HWHM) of the renormalized state. This Σ_i only vanishes at the uppermost valence state and at the lowest conduction state, i.e., for the lowest absorption edge (which can be either direct, like in GaAs, CdS, CuCl and GaN, or indirect, like in Ge, Si, diamond and GaP). The absorption spectra corresponding to this edge can, therefore, be very sharp at low T [42]. Diagram (ii) represents the second-order electron-phonon perturbation Hamiltonian, i.e., the second derivatives of the Hamiltonian with respect to the vibrational displacements, taken only to first order in perturbation theory and thus leading to simple frequency shifts without imaginary energy components. It is not uncommon to find in the older literature frequency renormalizations corresponding to only one of the diagrams in Fig. 1. Since 1983, however, both components of the electron-phonon interaction have been usually evaluated and added [9,44].

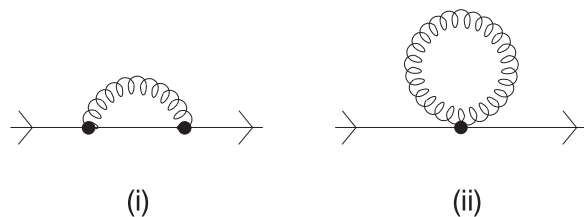


Figure 1: Electron-phonon interaction terms that contribute to the renormalization of electronic states. (i) Fan terms corresponding to a complex self-energy. (ii) Debye-Waller terms leading to a real energy correction.

For elemental crystals the electronic energy shift induced by the term (ii) can be written as [9]:

$$\Delta\omega(T) = \sum_{n,\mathbf{q}} \frac{A_{DW}(n,\mathbf{q})}{\Omega(n,\mathbf{q})M} (2n_B + 1) \quad (6)$$

where $A_{DW}(n,\mathbf{q})$ is a real coupling constant specific to the electronic state under consideration and M the mass of the element at hand. In a \mathbf{k} -dependent pseudopotential representation,

Eq. (6) can be evaluated by multiplying the pseudopotential form factors by Debye-Waller factors [30]. This procedure reduces simply to performing band structure calculations with two sets of pseudopotentials, the bare one and that screened by temperature-dependent Debye-Waller factors. This is the reason why calculations are often performed, using *Occam's razor*, only for the (ii) terms, neglecting (i) [45], a procedure known nowadays to be unjustifiable. Actually, when using a pseudopotential or any kind of truncated Hamiltonian for the calculation, the separate real parts of (i) and (ii) do not have an independent meaning as they depend on the type of truncation at hand. Only their sum is physically meaningful.

The self-energy terms (i) of Fig. 1 can also be represented by an equation of the type of Eq. (6) with a complex coupling constant $A_{SE}(n, \mathbf{q})$ which corresponds to the typical second-order perturbation expressions, with squared matrix elements in the numerator and an energy denominator with an infinitesimal imaginary convergence term in it [9]. Its numerical evaluation is considerably more complicated than that of the Debye-Waller terms (ii), since it involves not only a sum over all phonon states, but also one over intermediate electronic states. The early analytical calculation by Fan [8], while pioneering, is therefore highly unreliable.^a Fan suggested a procedure to relate the (i) to the (iii) terms by assuming parabolic band edges in order to perform analytically the integration of Eq. (6). Two parameters, corresponding to the deformation potentials of the conduction and valence band edges, are then introduced. Their difference determines the (iii) terms whereas the properly weighted difference of their squares determines the (i) terms. The (ii) terms are ignored. This procedure, if correct, allows the separate determination of the hydrostatic deformation potentials of the valence and conduction bands as done in Ref. [43]. However, as already mentioned, the results of this procedure are not trustworthy.

Note the similarity between Eqs. (6) and (4). At temperatures higher than the average phonon frequency (sometimes called the Debye frequency), they become linear in T . This fact, which follows from our assumption of terms only up to second order in the corresponding perturbation expansion [8,9,44] is often corroborated by experiments up to temperatures somewhat below the melting point. For $T \rightarrow 0$, Eqs. (4) and (6) tend to finite contributions to the zero-point renormalization. The high-temperature expansion of Eq. (6) can be written as

$$\Delta\omega = \frac{1}{M} \left[\left\langle \frac{A}{\Omega} \right\rangle + 2 \left\langle \frac{A}{\Omega^2} \right\rangle T \right], \quad (7)$$

where the brackets represent average values. A similar expression applies to the high-temperature limit of Eq. (4). Considering the fact that in elemental crystals all frequencies Ω are proportional to $M^{-\frac{1}{2}}$, we conclude from Eq. (7) that in the high- T limit $\Delta\omega$ is independent of M (classical limit). For $T \rightarrow 0$ (quantum limit)

$$\Delta\omega \propto M^{-\frac{1}{2}}. \quad (8)$$

Equations (7,8) apply to all three components (i, ii, iii) of $\Delta\omega$. If we are able to observe a linear region in $\Delta\omega(T)$ at large T , the extrapolation of this asymptotic linear behavior to $T = 0$ enables us to estimate the zero-point renormalization of the corresponding critical point (CP) energy $\Delta\omega(T = 0)$.

Figure 2 displays the temperature dependence of the energy of the lowest (indirect) gap of germanium and the linear high- T asymptote extrapolated to $T = 0$ [46,47]. This extrapolation leads to the estimate $\Delta\omega(T = 0) = -53$ meV for the zero-temperature phonon renormalization

^aFan obtained reasonable agreement with experimental data available to him, in spite of not having considered the (ii) terms. This is not unusual in the case of theories constructed so as to explain extant experimental results.

of the gap energy at 0 K. Using Eq. (8) we can estimate a difference of 2.2 meV between the corresponding gaps of ^{76}Ge and ^{70}Ge , which compares well with the measured value of 2.2 meV [48]. Figure 2 displays not only the experimental points for $E_g(T)$ but also the calculated sum of the (i) and (ii) contributions (dashed line) and this sum plus the thermal expansion contribution (iii) (solid line) [46].

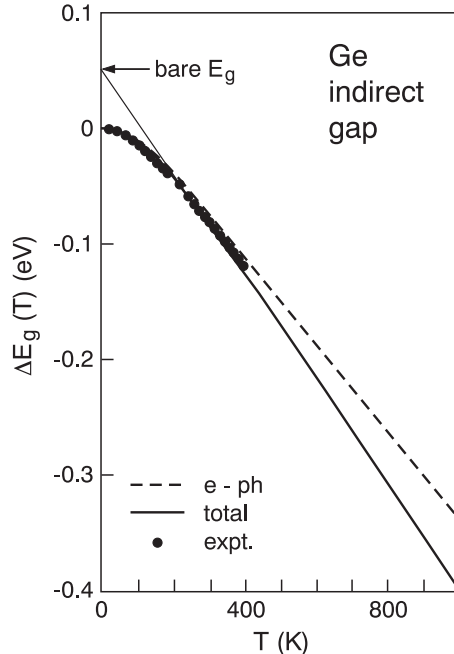


Figure 2: Temperature dependence of the energy of the lowest indirect gap of germanium. The dashed line represents the effect of electron-phonon interaction. The thick line represents this effect plus the thermal expansion effect. The thin line represents the asymptotic extrapolation to the bare gap at $T = 0$. The points are experimental [46].

We should recall that the direct gap E_0 of Ge is not its lowest gap, there being the indirect E_g gap ($\Gamma - L$) just discussed about 150 meV below. Hence, the zero-point self-energy of the direct gap E_0 should have an imaginary part which should be small because this gap is not far from being the lowest. From Fig. 1 in Ref. 48 we estimate $-\Sigma_i \simeq 0.5$ meV at $T \simeq 0$ K, much smaller than $\Sigma_r = 70$ meV [48].

We have, thus far, lumped all contributions (i), (ii), (iii) to Σ into a single one. In order to illustrate that the three contributions have the same asymptotic behaviors, we display in Fig. 3 the measured change in lattice parameter $a_0(T)$ of diamond with temperature (related to $\Delta V(T)$ in a straightforward way) [49]. The asymptotic linear extrapolation leads to a zero-point renormalization $\Delta a_0/a_0 = 0.374$ which, using Eq. (8), allows us to predict a difference between the lattice constants of ^{12}C (larger) and ^{13}C equal to 1.5×10^{-4} , in excellent agreement with the experimental results and *ab initio* calculations [50,32]. Notice that the one-oscillator fit of Fig. 3 leads to an average phonon temperature $\Omega = 1460\text{K}$, which compares well with the corresponding value for the specific heat (1450K [3]). The three oscillator fits of [37] leads to a dominant frequency $\Omega = 2137\text{K}$, rather close to that of a two-oscillator fit of the specific heat (1884 K [2,3]).

Concerning the dependence of physical parameters on isotopic mass, in this section we have confined ourselves to elemental crystals: only the mass of one element appears in Eqs. (7,8). In the case of binary or more complex crystals, that dependence is different for each one of

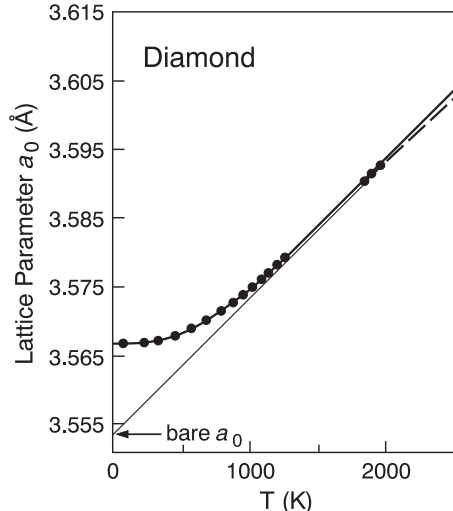


Figure 3: Lattice parameter a_0 of natural diamond vs. temperature. The points represent schematically the experimental data (up to 2000K). The thin line is the high temperature asymptote which extrapolates to the bare a_0 for $T \rightarrow 0$ (horizontal arrow). The thick curve represents a three-oscillator fit whereas the dashed curve (only plotted for $T > 2000\text{K}$) corresponds to a one-oscillator fit. See [37] and text.

the constituent masses and Eq. (7) becomes considerably more complicated. The experimental [51] and theoretical [52] information concerning dependences on isotopic masses for compound semiconductors is rather scarce. It can, nevertheless, be very interesting. In the case of the copper halide CuCl, for instance, the lowest gap (E_0) increases with increasing Cl-mass (a trend which agrees with Fig. 2) whereas it anomalously decreases with increasing Cu-mass [51,52].

3 Approximate Expressions for the Dependence of CP Energies on Temperature

A number of empirical [53] and semiempirical [54–56] analytical expressions have been proposed to represent the measured $\Delta\omega_0(T)$ and the corresponding imaginary part of the self-energy. The most popular fully empirical expression, proposed by Varshni, [53] is:

$$\Delta\omega_0(T) = \frac{\alpha T^2}{\beta + T}. \quad (9)$$

At high T , Eq. (9) becomes linear in T , in agreement with the discussion of Sect.2. For $T \rightarrow 0$, however, it becomes quadratic in T , leading to a stronger variation with T than observed experimentally (see Fig. 2 in Ref. 56 for GaAs).

The semiempirical expressions usually capitalize on the statistical factors $(2n_B + 1)$ which appear in Eqs. (4) and (6), replacing them by average values. In Ref. 54 one average value, corresponding to a single Einstein oscillator as used in the theory of the specific heat [1], is employed. In Refs. 43 and 55 two oscillators are used, paralleling the improved theory of the specific heat of Nernst and Lindemann [2]. Like in the case of the specific heats [3], electronic self-energies due to electron-phonon interaction at low T deviate from the single oscillator behavior. Two oscillators [2,55] improve matters a bit but, n_B implying an exponential dependence on T , cannot reproduce the T^3 behavior found experimentally for the specific heat

of insulators. It is easy to prove that Eqs. (4), as well as (6), also lead to a low temperature behavior proportional to T^3 . This is accomplished in Eq. (4) by replacing the sum by an integral over energy, which requires the introduction of the density of phonon states, proportional to Ω^2 at low T . Switching to the dimensionless variable of integration $\xi = \Omega/T$ leads to the factor T^3 that we are looking for.^b In order to obtain the same factor with Eq. (6), we need some additional reasoning. We must consider the fact that translational invariance requires that the electron-phonon coupling constant vanishes for $\Omega \rightarrow 0$: long wavelength acoustic phonons are equivalent to a uniform translation which does not couple to the electronic states. Hence, a factor of Ω^2 appears in A_{DW} and A_{SE} . The same factor of T^3 is then obtained in Eq. (4) for $T \rightarrow 0$. We thus see that Eq. (9), leading to $\Delta\omega_0(T) \propto T^2$ for $T \rightarrow 0$, cannot be correct either. Several attempts to remedy this problem, using empirical expressions, appear in the works of Pässler [56]. We illustrate them in Fig. 4 for the indirect gap of Si. The experimental points fall above the single oscillator fit of Ref. 54, as expected. Also as expected, the fit with Eq. (9) falls well above the single oscillator fit of Ref. 54. An excellent fit is obtained with the four-parameter expression:

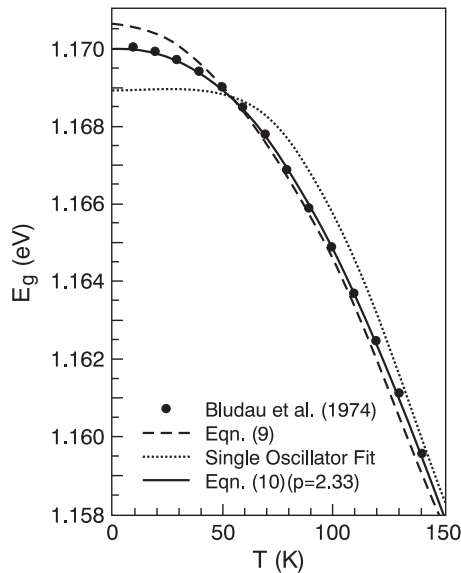


Figure 4: Temperature dependence of the indirect gap of silicon $E_g(T)$. The points are experimental, the solid line represents a fit with Eq. 10. Other details are given in the figure and in the text. Adapted from [56].

$$E_g(T) = E_g(0) - \frac{\alpha\Theta}{2} \left[{}^p\sqrt{1 + \left(\frac{2T}{\Theta}\right)^p} - 1 \right] \quad (10)$$

for $p = 2.33$. Equation (10) leads to a linear T -dependence for $T \gg \Theta$, as it should. Obtaining a good fit with an empirical or semiempirical expression is very helpful for the precise determination of the linear asymptotic behavior which, as discussed in Sect. 2, can be used to find the zero-point gap renormalization.

^bNote that if $\gamma_n(\mathbf{q})$ undergoes the changes in sign mentioned above, the range of T^3 behavior for the thermal expansion at low temperatures will be rather small. However, as already mentioned, these changes in sign make the behavior of $V(T)$ vs. T very flat at low T , thus improving the overall quality of single oscillator fits, although they cannot describe the resulting non-monotonic behavior of the expansion coefficient for $T \rightarrow 0$.

An excellent fit to $E_g(T)$, such as that provided by Eq. (10) (with $p = 2.33$, $\Theta = 405.6$ K, $\alpha = 0.3176$ meV \cdot K $^{-1}$), can be used to circumvent the problem of determining the high temperature asymptote, and thus the zero-point renormalization mentioned above. Using Eq. (10) we obtain for the $T = 0$ renormalization:

$$\Delta E_0(T = 0) = -\frac{\alpha\Theta}{2}. \quad (11)$$

Replacing into Eq. (11) the value $\alpha = 0.3176$ meV \cdot K $^{-1}$, and $\Theta = 405.6$ K given in [48], we find $\Delta E_0(T = 0) = -64$ meV for the indirect gap of Si. From this value of the zero-point renormalization one can estimate with Eq. (8) the isotope shift of the indirect gap of silicon, between natural silicon ($M = 28.0856$) and isotopically pure ^{28}Si , to be 0.12 meV, in good agreement with the experimental results (0.094 meV) [42].

We show in Table I the values of the zero-point renormalization of the lowest gaps (plus the lowest *direct* gap of Ge) of several diamond and zincblende-type semiconductors, together with the corresponding values of dE/dM . The first column under $\Delta E(T = 0)$ and dE/dM represents experimental data obtained by the linear extrapolation technique and by isotopic substitution, respectively (an exception is the case of diamond, for which the calculated value of $\Delta E(T = 0)$ [44] is given). The available experimental data for diamond do not allow a reliable extrapolation to $T = 0$, the experimental value of dE_g/dM listed in Table I is from [57]. The numbers in the second column under $\Delta E(T = 0)$ (and dE/dM) were estimated from the “experimental” values of dE/dM (and $\Delta E(T = 0)$) using the $M^{-\frac{1}{2}}$ dependence, as discussed above. The values of $\Delta E(T = 0)$ are rather similar for most materials in the table, with the exception of those for diamond, which are very large, and the rather small ones listed for the copper halides (to be discussed in Sect. 4.2). We note that several electron-phonon coupling constants of diamond are known to be considerably larger than those for other zincblende-type semiconductors [58], a fact which we conjecture it arises from the absence of p-like electrons in the core of the carbon atoms. Correspondingly, the measured dE_g/dM is also rather large for diamond [57].

4 Lowest Direct Gap E_0 of compound Semiconductors: Temperature and Isotope Effects

Information on the temperature dependence of the lowest gaps of many semiconductors can be found in standard compilations of semiconductor properties (e.g., the Landoldt-Börnstein Tables and Ref. [47]). We shall discuss in this section a few cases for which isotopic data are also available.

4.1 GaAs and ZnSe

The temperature dependence of E_0 for GaAs is rather similar to that for germanium, as expected from the similarity in their band structures and lattice dynamics. The parameters for the best fit with Eq. (10) are $\Theta = 226$ K, $\alpha = 0.473$ meV \cdot K $^{-1}$, $p = 0.251$ [59]. Using these parameters one predicts with Eq. (11) $\Delta E_0(T = 0) = -53$ meV, a value very close to that given in Table I for Ge. Unfortunately, arsenic has only one stable isotope (^{73}As) so that only the effect related to the two isotopes of Ga, ^{69}Ga and ^{71}Ga , can be experimentally investigated. Common sense, and also pseudopotential calculations [52], suggest that the effect of varying the Ga mass should be nearly the same as that of varying the As mass (per unit atomic mass). The effect

of the ^{69}Ga - ^{71}Ga substitution, realized experimentally, can thus be predicted by dividing the prediction of Eq. (8) for germanium by 2. We thus predict for the derivative of E_0 with respect to the Ga mass:

$$\frac{\partial E_0}{\partial M_{Ga}} = \frac{1}{4 \times 70} \times 53 = 0.19 \text{ meV/amu} \quad (12)$$

This value is a factor of two smaller than the measured one (0.39 meV/amu) and also than the value obtained from the pseudopotential calculations (0.43 meV/amu) [52]. The reason for this discrepancy is not known but it may lie on having taken too small a temperature range for the fit in Ref. [59]. Indeed, if we use the data for $E_0(T)$ given in Fig. 2 of Ref. [47] for GaAs we find $\Delta E_0(T = 0) = -90$ meV, a value which leads to dE/dM_{Ga} , in rather good agreement with the experimental result (see Table I).

For ZnSe, the linear extrapolation of $E_0(T)$ gives a zero-point renormalization $\Delta E_0(T = 0) = -65$ meV [52]. Pseudopotential calculations [52] yield a stronger electron-phonon contribution to the isotope effect for Se ($\partial E_0/\partial M_{Se} = 0.26$) than for Zn ($\partial E_0/\partial M_{Zn} = 0.19$),^c although the difference is compensated, at least partially, by the corresponding thermal expansion effects [33,52]. The measured values of $\partial E_0/\partial M_{Zn} = 0.214$ and $\partial E_0/\partial M_{Se} = 0.216$ are indeed nearly equal (see [51,60] and Table I). The value estimated with Eq. (8) assuming that both derivatives are equal is 0.24 meV, in reasonable agreement with the experimental results.

Notice that the thermal expansion contribution $\Delta E_{th}(T = 0)$ shown in Table I for GaAs is about 40% of the total gap renormalization $\Delta E_0(T = 0)$ and has the same sign. In the case of GaP, however, the thermal expansion contribution to the indirect gap is only 4% of the total effect and has the opposite sign. This apparent anomaly is related to the large value and the negative sign of the deformation potential of direct E_o gaps and the small value plus sign reversal which takes place for the $\Gamma \rightarrow \Delta$ indirect gaps E_g . Similar effects can be seen in Table I for $\Delta E_0(T = 0)$ of Ge as compared with $\Delta E_g(T = 0)$ of Si. For the indirect gap of germanium E_g , the sign of the thermal expansion renormalization is the same as that of E_0 and its absolute value is somewhat smaller (25%) as corresponds to a $\Gamma \rightarrow L$ indirect gap.

4.2 The cuprous halides

CuCl, CuBr and CuI (I-VII compounds) crystallize, under normal conditions, in the zincblende structure. However, when compared with their group IV, III-V and II-VI counterparts, they display a number of anomalous properties [52,60,65] which are usually attributed to a strong hybridization of the halogen p valence bands with the 3d electrons of copper. Among these properties we mention, as relevant to the present paper, the increase in E_0 with increasing T observed for CuCl and CuBr.^d

Figure 5 displays the anomalous temperature dependence of the E_0 gap of CuCl [51]. The experimental points show an increase in gap energy with increasing temperature, with an increasing slope at low T that begins to decrease at ~ 100 K and seems to saturate at ~ 300 K. This behavior can be phenomenologically interpreted by means of a two-oscillator fit [2], provided one assumes that the two oscillators give electron-phonon contributions of opposite signs: The lower frequency oscillator, most likely related to Cu vibrations, contributing a positive $\Delta E_0(T = 0)$ and the high frequency one, related to Cl, giving a negative contribution. These opposite signs agree with those determined experimentally for the derivatives of E_0 with respect to the copper

^cNote that this trend continues for CuBr where $\partial E_0/\partial M_{Cu}$ even becomes negative [51]

^dFor CuI E_0 decreases only very slightly between 0 K and room temperature [65,66].

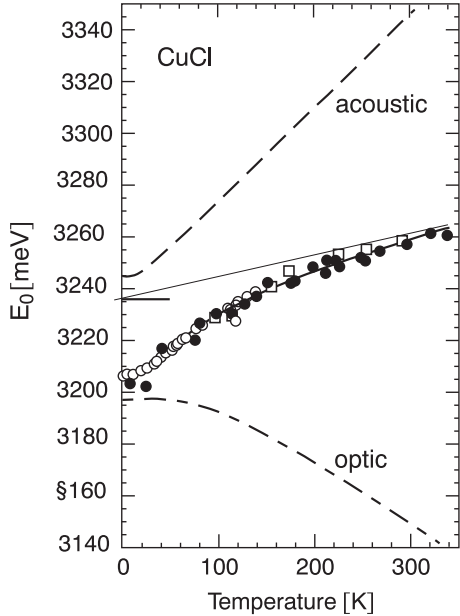


Figure 5: Temperature dependence of the Z_3 exciton energy (equivalent to that of the E_0 direct gap) of CuCl. The points are experimental, the thick solid curve represents a two-oscillator fit (acoustic and optic) while the thin line indicates the linear asymptote. From [51].

and chlorine masses ($\partial E_0/\partial M_{Cu} = -0.076$ meV/amu, $\partial E_0/\partial M_{Cl} = +0.36$ meV/amu, see Fig. 6.) [51].

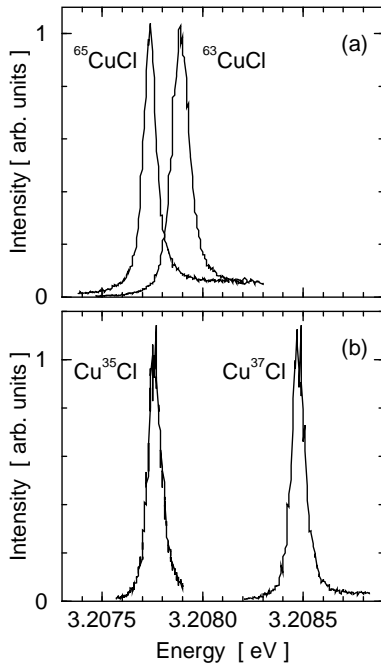


Figure 6: Two-photon absorption in the region of the longitudinal exciton (LE1) in isotopically modified CuCl measured at 2K. The isotopic shifts shown in this figure are expected to correspond to those of the direct gap $E_0 + \Delta_0$, which should be nearly the same as those of E_0 . Notice that the shifts with increasing mass are negative (i.e., anomalous) for Cu and positive for Cl [51].

The question arises as to whether the anomaly just mentioned is due to the electron-phonon interaction or to the thermal expansion term. Fortunately, the deformation potential $\partial E_0/\partial \ln V$, and also the thermal expansion, are very small and the corresponding effect can be neglected for CuCl and approximately neglected for CuBr, see Table I. The anomalous contribution of Cu, and that of the halogen, must then be due mainly to electron-phonon interaction.

The two-oscillator contributions to $\Delta E_0(T)$ are labeled “acoustic” and “optic” in Fig. 5. The anomalous acoustic contribution has been attributed in Ref. 51 predominantly to the Cu vibrations, the optic contribution, with the usual sign, to chlorine. An excellent fit to the experimental data is obtained when adding both contributions. The horizontal line represents the

bare gap as obtained from the two-oscillator fit. A thin straight line represents the asymptotic behavior at high T and extrapolates to the bare gap for $T = 0$.

A similar anomalous behavior of $E_0(T)$ and $\partial E_0/M_{Cu}$ is found for CuBr [51,65,66]. A negative $\partial E_0/\partial M_{Cu}$ is also found for CuI.^e However, at least below 300 K for CuI, $E_0(T)$ decreases with increasing T [65]. This case is in the process of being analyzed [66].

5 Higher Critical Points: Dependence on Temperature and Isotopic Mass

We have labeled as E_0 the lowest direct critical point (i.e., energy gap) of a germanium and zincblende-type semiconductor. In all cases discussed, E_0 is found around the Γ -point (center) of the Brillouin zone. If it is the absolute minimum of all transition energies, including indirect ones (e.g., for GaAs, see Fig. 7, [67]), the corresponding Σ_i vanishes.^f If not, a finite value of Σ_i is expected (e.g., Ge, $-\Sigma_i = 0.5$ meV at $T = 0$, see Sect. 3). The E_0 CP at Γ is split by spin-orbit interaction, the second component being known as $E_0 + \Delta_0$. A finite value of Σ_i is expected for this second component since it is not the lowest: it is induced by the electron-phonon interaction between the corresponding valence state at the Γ point and the top valence band of Γ , at nearly the same energy [67–70] ((i) terms of Fig. 1). In the case of GaAs, $-\Sigma_i$ for $E_0 + \Delta_0$ has been found to be 6 meV at 2K [69,70]. The behavior of $-\Sigma_i$ with increasing temperature can be estimated by multiplying 6 meV by $2\langle n_B \rangle + 1$, $\langle n_B \rangle$ being the Bose-Einstein factor for the appropriate average phonon frequency.

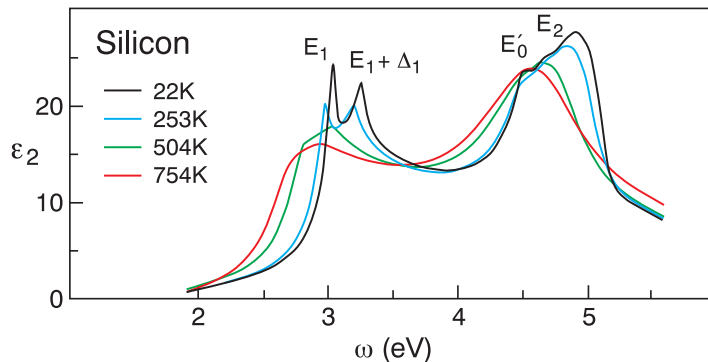


Figure 7: Spectra of the dielectric function $\epsilon_2(\omega)$ of GaAs ellipsometrically measured at several temperatures. Notice the critical points labeled E_1 , $E_1 + \Delta_1$, E'_0 , and E_2 . From [67].

E_0 and $E_0 + \Delta_0$ correspond to optical absorption coefficients of the order of 10^4 cm^{-1} ($\epsilon_2 \simeq 1$). With increasing photon energies the absorption coefficient rises to a maximum near 10^6 cm^{-1} : The corresponding CP is labeled E_2 . The $\epsilon_2(\omega)$ spectrum of GaAs in the region of strong electronic absorption (1.5 to 5.5 eV) is shown in Fig. 7 for several temperatures. The strongest feature corresponds to the E_2 CP's: it red-shifts and broadens strongly with increasing T . Another feature, labeled E'_0 , corresponds to transitions between the $\Gamma_{25'}$ valence band and the Γ_{15} conduction band states [67].

^e Unfortunately, iodine has only one stable isotope (^{127}I).

^f Note, however, that a broadening of the indirect absorption edge of natural (i.e., isotopically mixed) Si has been recently discovered. It disappears for isotopically pure ^{28}Si and thus can be attributed to isotopic disorder [42].

We display in Fig. 8 $\epsilon_2(\omega)$ spectra measured for GaAs at 20 and 300 K (from Fig. 7) and compare them with recent *ab initio* calculations of Rohlfing and Louie [12], one of the calculated spectra (dashed line) without electron-hole (exciton) interaction. The measured spectra display clearly the spin-orbit splitting of the E_1 transitions ($E_1 - E_1 + \Delta_1$). The spin-orbit interaction was not included in the calculations in order to reduce (by a factor of $2 \times 2 = 4$) the size of the Hamiltonian matrix. The calculations include, however, an artificial broadening $\Gamma \simeq 0.10$ eV so as to smooth out the limited \mathbf{k} -space integration mesh. This is the reason why the calculated $E_1 - E_1 + \Delta_1$ structure, in principle not including lattice vibrations, is broader than that measured at 20K. Unfortunately, because of the single isotope nature of arsenic (^{73}As) and the rather small mass difference between the two isotopes of Ga (^{69}Ga , ^{71}Ga), the experimental accuracy does not allow for an extrapolation of the $\epsilon_2(\omega)$ data to infinite isotopic masses, a procedure which would be desirable so as to compare measured with calculated spectra. In the case of Ge, however, the isotopic mass range available is much larger (^{70}Ge – ^{76}Ge). Moreover, one gains an additional factor of 2 (with respect to GaAs) because for Ge both atoms in the primitive cell can be isotopically substituted. Nevertheless, such an isotopic extrapolation procedure, which we believe to be possible but difficult, has yet to be performed.

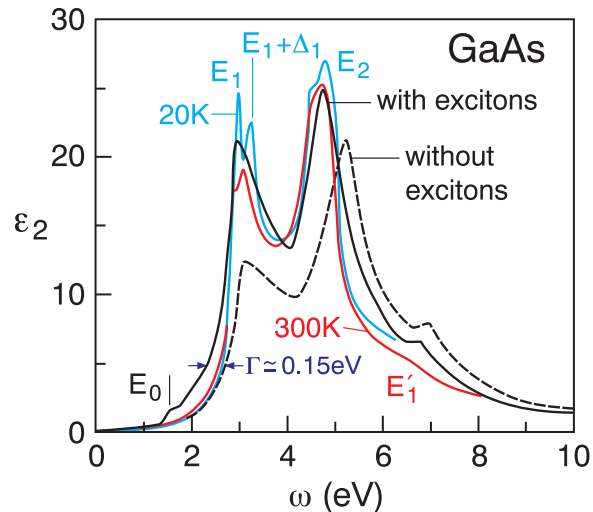


Figure 8: Spectra from Fig. 7 at 20K (blue) and 300K (red) compared with the calculations of Rohlfing and Louie [12] with (thick solid line) and without (dashed line) excitonic interactions but without spin-orbit coupling. The calculations include an *ad hoc* Lorentzian broadening of 0.15 eV. Notice the enhancement of the E_1 and $E_1 + \Delta_1$ peaks induced by the excitonic interaction.

We shall discuss here in some detail the temperature and isotope effects of the E_1 and $E_1 + \Delta_1$ features of Ge and Si. They correspond to transitions between the top valence bands and the bottom conduction band along the $\langle 111 \rangle$ directions (labeled as Λ). Their splitting, 190 meV for Ge, is due to spin-orbit interaction. Similar features are observed for all materials of the germanium-zincblende family [68]: A red shift (Σ_r) and a broadening with increasing temperature.

5.1 The E_1 and $E_1 + \Delta_1$ critical points of germanium: temperature and isotope effects

Rönnow *et al.* [71] were able to determine with a remarkable accuracy the dependence of $\Sigma(T=0)$ on isotopic mass for the E_1 and $E_1 + \Delta_1$ CP's of germanium. We show in Fig. 9 the third derivative of ellipsometrically determined spectra of $\epsilon_1(\omega)$ and $\epsilon_2(\omega)$ for three germanium wafers with different isotopic compositions measured at 30K. It is easy to see in this figure that the E_1 and $E_1 + \Delta_1$ curves shift to larger frequencies with increasing isotopic mass, in agreement with the results found for the E_g and E_0 critical points (Table I). The critical point parameters E_1 , $E_1 + \Delta_1$, and Γ (HWHM) obtained from the spectra of Fig. 9 are plotted in Figs. 10 and 11 versus isotopic mass. In spite of the considerable scatter of the experimental points, a clear trend is apparent: E_1 , $E_1 + \Delta_1$, and even their difference Δ_1 , increase with increasing mass. The solid lines in Fig. 10 are fits to $E = E_\infty + BM^{\frac{1}{2}}$, i.e., to the prediction of Eq. (8). These fits enable us to determine the bare values of the critical points E_∞ ; they are listed in Table II. Notice that the spin-orbit splitting Δ_1 shows a slight tendency to increase with increasing mass, surely a result of the electron-phonon interaction; quantitative calculations of this increase are not available.

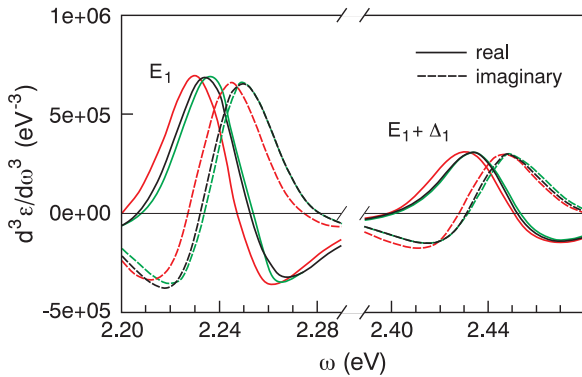


Figure 9: Third derivative with respect to photon energy of the dielectric function of natural Ge in the vicinity of the E_1 and $E_1 + \Delta_1$ transitions. The solid lines are fitted to the experimental data using analytical line shapes. Red curves: ^{70}Ge , black; natural Ge, green; $^{75.6}\text{Ge}$, [71].

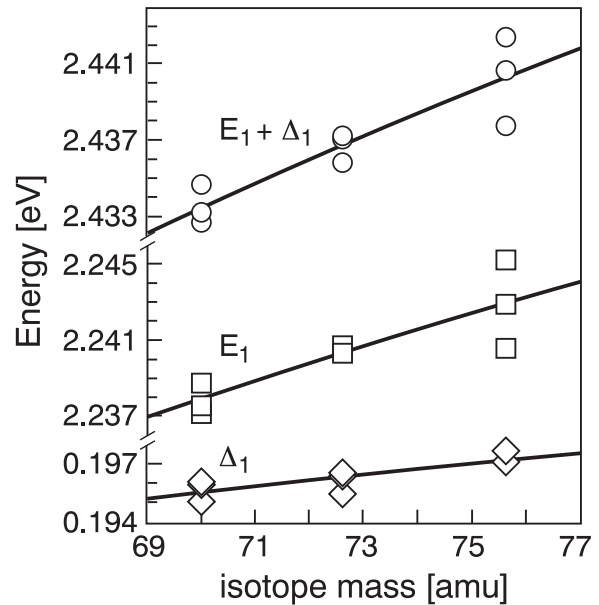


Figure 10: Energies of the E_1 and $E_1 + \Delta_1$ transitions in Ge, vs. isotope mass. Also shown is the dependence of the spin-orbit splitting, Δ_1 , on isotope mass. The solid lines are fits to $E = E_\infty + BM^{-\frac{1}{2}}$ (see [71]).

Figure 11 displays the decrease in the Lorentzian HWHM parameters of the E_1 and $E_1 + \Delta_1$ critical points of germanium observed with increasing isotopic mass. The solid lines are fits with the equation $\Gamma = \Gamma_\infty + BM^{-\frac{1}{2}}$, based also on Eq. (8), except that a small intercept Γ_∞ ($\simeq -6$ meV) allowed us to improve the fit. This intercept, if meaningful, would represent a “natural width” which would be present even when the atoms do not vibrate. It could be due either to crystal imperfections, among them the truncation at the surface, or, alternatively, to inadequacies in the line shape used to fit the experimental spectra. In Ref. 71 logarithmic singularities were used (see Eq. 4 in [71]) which correspond to two-dimensional interband critical

points. Excitonic effects may contribute a small *negative* Γ_∞ to the fitted $\Gamma(M)$ as also may the lowered dimensionality induced by the surface. The fitted value of B is 350 ± 90 meV/amu, in remarkably good agreement with band structure based calculations (310 meV/amu [44]).

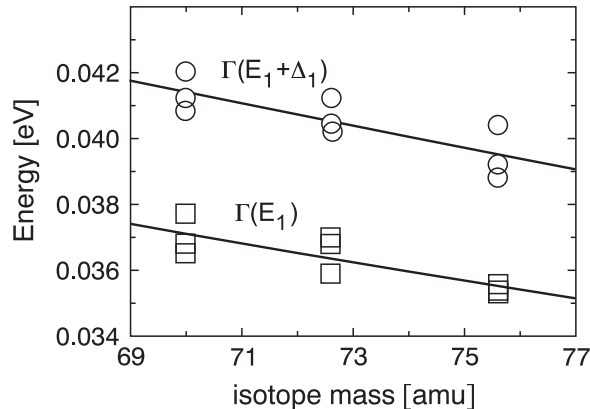


Figure 11: Lorentzian widths $\Gamma = -\Sigma_i$ of the E_1 and $E_1 + \Delta$ transitions of germanium vs. isotopic mass. The points are experimental. The lines represent fits to $\Gamma = \Gamma_\infty + BM^{-\frac{1}{2}}$ [71].

5.2 The E_1 critical points of silicon: temperature and isotope effects

Work similar to that described in Sect.5.1 for germanium has been performed for silicon by Lastras, *et al.* [26] using ^{28}Si , ^{30}Si and natural silicon ($M = 28.09$). Because of the small effects involved, the fits to the experimental lineshapes were performed with an elaborate, highly accurate Fourier transform technique [72]. The analysis of the data is further complicated by the inability to resolve the spin-orbit splitting Δ_1 (for $S_i, \Delta_1 \simeq 30$ meV), and the near-degeneracy of the E_1 CP's with the critical point E'_0 . Therefore, it was not possible to obtain data for the dependence of Σ_i on isotopic mass. The width of the E_1 transitions measured directly at $T = 10$ K is about 70 meV [73], a value somewhat larger than that found for the other materials under discussion. The value of $\Sigma_r(T = 0)$ obtained from the isotope shifts is 118 ± 22 meV, somewhat larger than the calculated value (71 meV) [74] and much larger than the value extracted from the measured temperature dependence of the E_1 transition (39 ± 13 meV) [73]. The discrepancy may be due to the complex nature of these transitions, as mentioned above.

We display in Fig. 12 the results of a recent *ab initio* calculation of $\epsilon_2(\omega)$ for silicon, performed both with (solid black line) and without (dashed line) excitonic interaction [14], compared with spectra measured ellipsometrically at 20 and 300K [73]. This figure emphasizes the importance of comparing calculations performed for static atoms with measurements at the lowest possible temperatures: the height of the E_1 peak measured at 20K agrees rather well with the calculated one. The calculated peak is, however, broader than the measured one. This is a trivial effect of having introduced in the calculation an artificial Lorentzian broadening parameter of about 100 meV. The calculated E_1 structure is of obvious excitonic nature since it goes down dramatically in strength if excitonic interaction is not included. It peaks 100 meV higher than that measured at 20K. While 100 meV is about the accuracy claimed for *ab initio* calculations, it is tempting to speculate, in view of the results for $\Delta E_1(T = 0)$ given in Table II, that the red shift of 100 meV found in the experimental spectrum with respect to the calculated one is due to the zero-point renormalization by the electron-phonon interaction.

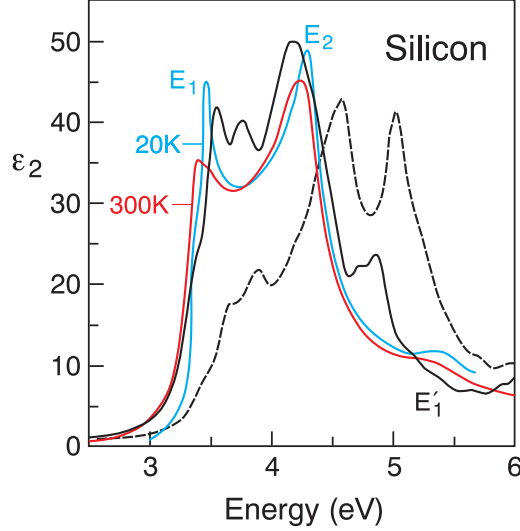


Figure 12: Ellipsometric spectra of $\epsilon_2(\omega)$ for silicon [75] at two temperatures compared with the calculations of Albrecht *et al.* [14] with (solid black line) and without (dashed line) excitonic interaction. Note that the peak calculated at 3.8 eV does not appear in the experimental data and thus it is to be regarded as spurious, possibly due to the coarse \mathbf{k} -space interaction mesh.

There has been some controversy concerning the peak exhibited by the black solid curve of Fig. 12 at 3.8 eV. While in the original publication [14] it was claimed that this peak corresponds to a well-established experimental feature, Fig. 12 contradicts this claim: It seems that the 3.8 eV feature is simply an artifact of the coarse mesh used for the calculation [25,75].

6 Linear Optical Response Related to Surface States: Effects of Electron-Phonon Interaction

There have been in recent years a large number of investigations of the response of electronic surface states to near-ir and visible light. This response is rather weak and can best be measured in a differential way which involves either subtracting the responses to two inequivalently polarized light beams, or letting the surface states disappear through passivation (e.g., oxidation [31]). Even so, measurements in uhv are difficult and time consuming. Consequently, only few experimental investigations of the temperature dependence of the corresponding spectra have been published [31,77,78]. These investigations are mainly concerned with the gap between filled and empty electronic surface states of cleaved [111] silicon surfaces. For a critical discussion see Ref. 79.

The spectra of 2×1 [111] silicon surfaces cleaved in vacuum consist of a strongly polarized (for $\mathbf{E} \parallel [1\bar{1}0]$, no response for $\mathbf{E} \parallel [\bar{2}11]$) peak centered at about 0.5 eV. This peak barely shifts with temperature, a fact which has been attributed in Ref. 79 to a compensation of the shifts induced by the various phonons involved.⁹

A red shift is, however, found for the low-frequency onset of this peak (0.43 eV at 20 K, 0.34 eV at 300 K [78]). The magnitude of this shift is similar to that found for the lowest absorption edge of many semiconductors (see Figs. 2 and 4). The onset of a weak absorption peak, however, cannot be very reliably measured and considerable differences exist among values reported for

⁹This is similar to the situation found for bulk CuI [65,66].

Si. Nevertheless, several attempts have been made to interpret the red shifts reported for the onset and the near lack of shift at the peak [79]. The authors of these attempts basically accept the latter fact and explain the shift of the onset as a broadening of the peak structure.

An interesting observation concerning the response of the 2×1 [111] silicon surface is the broadening with increasing temperature which can, of course, be attributed to electron-phonon interaction. We have seen in the previous sections that this broadening is proportional to T at high temperatures and becomes T -independent for $T \rightarrow 0$, at least for bulk semiconductors. In the case of surfaces one may argue that, because of the reduced dimensionality, the coupling to the surface electrons of individual surface phonons may be much stronger than in the bulk and therefore the lowest order perturbation theory which led to Eq. 6 may break down [80]. For the [111] silicon surface there is no convincing evidence for this to be the case.

It has been mentioned in Sect. 2.2 that, to lowest order in perturbation theory, both $\Delta E(T)$ and $\Gamma(T)$ are proportional to $\langle u^2 \rangle$ (u = phonon amplitude), i.e., to $2\langle n_B \rangle + 1$, where $\langle n_B \rangle$ is an average Bose-Einstein factor (Eq. (5)). This fact leads immediately to the linear dependence on T at high T which has been so profusely and fruitfully used throughout this article. The surface spectroscopist will, however, have found in the literature statements to the fact that the widths of spectral structures induced by transitions between electronic surface states are proportional to $[2\langle n_B \rangle + 1]^{1/2}$, i.e., to $T^{1/2}$ at high T [31,79]. This is a point where communication between surface and bulk physicists could have been better. The argument behind the linear- u dependence emphasizes the fact that the vibration, symmetric with respect to $u = 0$, slushes back and forth the frequency of the peak, thus producing a broadening proportional to u . Those familiar with the Debye-Waller theory will, however, realize that such a term generates only a broad background, not a renormalized band-structure preserving sharp critical points. The renormalization of the band structure contains, in the spirit of Fig. 1, only terms proportional to $2\langle n_B \rangle + 1$.

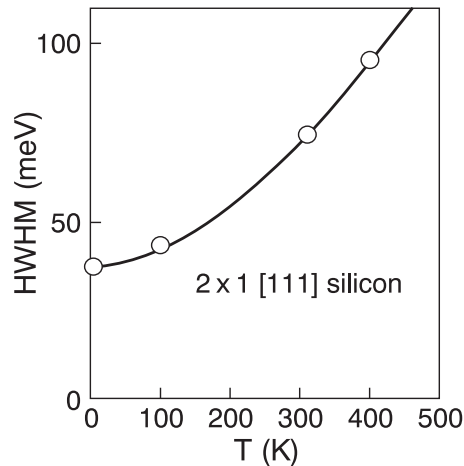


Figure 13: Widths (HWHM) of the spectral peak observed around 0.5 eV for a 2×1 -Si [111] surface at four temperatures. The three points above 100 K are from [31], that near $T = 0$ was recently communicated to us by the authors of [31]. The line through the points represents a fit with the function $[2n_B(\Theta/T) + 1] \times \Gamma(0)$ which led to $\Theta = 340$ K, a rather reasonable value for silicon.

Unfortunately, the only measurements vs. temperature of the width of the 2×1 Si [111] peak were reported solely for three temperatures [31] (see Fig. 13; a fourth point, close to $T = 0$, has been recently communicated to us by the authors of [31]) and they hardly possess enough information to refute experimentally the square-root hypothesis. In fact, they were presented

in [31] as supporting it. We have plotted in Fig. 13 these points vs. T and fitted them with a single-oscillator $2n_B + 1$ expression. The fit for an average frequency $\theta = 340\text{K}$, is quite satisfactory, slightly better than the square-root fit of Fig. 2 of [31].

7 Dependence of Other Physical Properties on Temperature and Isotopic Mass

The Bose-Einstein fits and measured temperature dependences of a wide variety of physical properties of semiconductors, in connection with linear asymptotic expansions, can also be used to estimate the zero-point renormalization of these properties and the corresponding isotope effects. In this section we briefly discuss the long-wavelength refractive index, the phonon frequencies and the elastic constants for elemental semiconductors. The semiempirical expressions used for the fits are basically the same as those discussed in previous sections for interband transition energies. However, the $M^{-\frac{1}{2}}$ dependence of the zero-point renormalizations, given in Eq. (8), must be modified depending on the type of property under consideration. This dependence still holds for the long wavelength refractive index since it is directly related to $\epsilon_1(\omega)$ and $\epsilon_2(\omega)$ (a straightforward calculation suffices to prove it).

In the case of phonon properties, such as phonon frequencies, the $M^{-\frac{1}{2}}$ dependence must be replaced by M^{-1} . This is easily understood. The diagram, corresponding to (ii), which represents an anharmonic renormalization of a phonon frequency, is obtained by replacing the horizontal electron propagators by curly phonon propagators. Hence, four phonon amplitudes come together at the vertex, giving a matrix element proportional to u^4 , i.e., to M^{-1} . For the elastic constants, proportionality to $M^{-\frac{1}{2}}$ obtains.

7.1 Long wavelength refractive index: temperature dependence and isotope effects

The temperature dependence of the long wavelength refractive index plays an important role in the tuning of optical and optoelectronic devices. Early theoretical work was concerned only with the temperature region in which the T -dependence is linear [45,81]. Recently, *ab initio* calculations over a broad temperature range, including the zero-temperature renormalization, have been performed [7]. Experimental results are given in [82] for diamond and in [7] for Si and Ge.

The following fitted expression is given in Ref. 82 for the long wavelength refractive index $n(T)$ of diamond.

$$n(T) = n_0 + \frac{A}{2} \left[2n_B(\Omega, T) + 1 \right] \quad (13)$$

where $\Omega = 711 \text{ cm}^{-1}$, $A = 0.19$ and $n_0 = 2.377$. This expression implies that the zero-point renormalization is $\Delta n(T = 0) = 0.085$, rather close to the value 0.07 obtained by linear extrapolation from Fig. 5 of Ref. 7. Note, however, that the value of Δn given in Table I of Ref. 7 is three times larger and thus must be erroneous, since inconsistent with Fig. 5 of that reference.

From the zero-point renormalization $\Delta n(T = 0) = +0.085$, the dependence on isotopic mass:

$$\left(\frac{\partial n_0}{\partial M}\right) = 4 \times 10^{-4} \text{ K}^{-1} \quad (14)$$

is obtained. It is slightly larger than the value $3 \times 10^{-4} \text{ K}^{-1}$ calculated in Ref. 7. Fabry-Perot interference fringes are a very accurate method to measure differences in refractive indices. They could be used to measure the coefficient of Eq. (14) by comparing two plane-parallel diamond wafers made out of ^{12}C and ^{13}C , respectively. The expected value of this coefficient, however, is so small that differences in the samples resulting from their fabrication, but due to reasons other than their isotopic mass, would be likely to obliterate the expected results. At this time it would also be very difficult to measure the corresponding derivatives of n_0 for Ge and Si which, nevertheless, can be easily obtained from the calculations in [7].

7.2 Anharmonic self-energy of phonons: effects of temperature and isotopic substitution

Although anharmonic self-energies can be found for all phonons in the dispersion relations, most of the information available concerns the Raman phonons, i.e., the optical phonons for $\mathbf{q} = 0$. In most cases analyzed in detail, the equivalent of the two terms in Fig. 1 (with the electron lines replaced by phonon propagators) suffice to explain the measured $\Sigma(\Omega)$ [10,83,84].

Let us first discuss the dependence of the phonon linewidth (HWHM = $-\Sigma_i$) of the equivalent of Fig. 1 for phonons. No contribution of the phonon-phonon equivalent of (ii) exists [85,86]. The contribution of (i) to Σ_i represents a decay of the phonon under consideration (frequency Ω , $\mathbf{q}=0$ for the Raman phonon) into two phonons, with frequency and wavevector conservation ($\Omega = \Omega_1 + \Omega_2$; $\mathbf{q} = \mathbf{q}_1 + \mathbf{q}_2$). In the case of Ge and Si excellent fits to the measured temperature dependence of the HWHM are obtained with the expression [85,86]:

$$\Gamma(T) = -\Sigma_i(T) = \Gamma_0 \left[1 + n_B(\Omega_1, T) + n_B(\Omega_2, T) \right] \quad (15)$$

where $\Omega_1 = 2\Omega_2 = 0.66\Omega$ (Ω_1 and Ω_2 correspond to LA and TA phonons at the edge of the BZ), and the zero-point renormalization $\Gamma_0 \simeq 0.5 \text{ cm}^{-1}$, which has indeed been shown to be proportional to M^{-1} .^h The energy conservation constraint $\Omega = \Omega_1 + \Omega_2$ is only required for the evaluation of Σ_i .

The frequency shift Σ_r , including the contribution equivalent to (ii), is obtained by summing over all possible *virtual* intermediate states, with ($\mathbf{q} = \mathbf{q}_1 + \mathbf{q}_2$) but without the requirement of energy conservation. However, because of the energy denominators which appear in the second-order perturbation expression corresponding to Σ_r , two phonons with $\Omega_1 + \Omega_2$ near Ω often give the dominant contributions to Σ_r . Hence, it is common to find in the literature fits to the measured $\Sigma_r(T)$ with Eq. (15) and the restriction $\Omega = \Omega_1 + \Omega_2$. Such a fit is found for silicon in Fig. 3 of Ref. 83. It leads to an estimate $\Sigma_r = -5.6 \text{ cm}^{-1}$ for the zero-point anharmonic renormalization of the phonon frequency of Si (bare frequency at $T = 0$ equal to 531 cm^{-1}). This zero-point renormalization, proportional to M^{-1} , decreases in absolute value by 0.39 cm^{-1} when replacing ^{28}Si by ^{30}Si .

^hSee Fig. 4 in Ref. 83, where the contribution of isotopic disorder to Γ has also been included. This contribution amounts to 0.035 cm^{-1} HWHM for a mixture of equal parts of ^{28}Si and ^{30}Si .

7.3 Elastic Constants

The temperature dependence of the elastic stiffness moduli $C_{11}(T)$, $C_{12}(T)$ and $C_{44}(T)$ has been measured for diamond [87], silicon [88], and germanium [88]. In spite of the temperature range, which was limited to T slightly below the Debye temperature, it has been possible to estimate the position of the linear asymptote required for the determination of the zero-point renormalization. As already mentioned, this renormalization is related to that of the long-wavelength acoustic phonons and turns out to be proportional to $M^{-\frac{1}{2}}$.

In Table I of [49] the values of the elastic constants, the estimated temperature renormalization and their logarithmic derivatives with respect to M , calculated by using the $M^{-\frac{1}{2}}$ dependence on mass, are displayed. No experimental data are available for these derivatives but, in spite of the small values involved, they may be measurable using the highly accurate ultrasonic propagation technique.

It is interesting to mention that a value of $\partial \ln C / \partial M = 5 \times 10^{-3}$ was reported in [89] for diamond. A point was made in that paper of the fact that correspondingly, ^{13}C diamond must be significantly harder than ^{12}C diamond. This $\partial \ln C / \partial M$ is about an order of magnitude larger than the value obtained from Table I of Ref. [49], which implies insignificantly harder ^{13}C diamond. In a following paper [90] an error in the interpretation of the experiments of [89] was corrected. This correction, and an estimate with a theoretical model, led to a value of $\partial \ln C / \partial M \leq 10^{-3}$, in agreement with the value given in Table I (3.5×10^{-4}).

8 Conclusions

We have discussed the renormalization of a broad range of physical properties of tetrahedral semiconductors by the electron-phonon interaction. These properties include the dielectric functions and the corresponding electronic transition energies (both bulk and surface contributions), the lattice parameter, the phonon frequencies and the elastic stiffness constants. Particular attention has been paid to the zero-point ($T = 0$) renormalizations, which can be changed by changing the isotopic masses. Semiempirical expressions representing these renormalizations vs. temperature have been given. Especially powerful for the interpretation of experimental results has been shown to be the determination of the asymptotic linear behavior vs. temperature at high temperature, either with the naked eye or, even better, from a fit to a well-founded analytical expression.

In this article we have only discussed elemental and binary semiconductors. A few cases involving materials with three different elements or more can be found in the literature. Of particular interest are the I-III-VI chalcopyrites containing as element either copper or silver (e.g., CuGaSe_2 [91], which is isoelectronic to ZnSe ; AgInSe_2 [92] isoelectronic to CdSe ; AgGaSe_2 [93]). These materials all exhibit anomalies in the temperature dependences of the gap which are reminiscent of those observed for the copper halides: at low T the gaps increase with increasing T , whereas they decrease at higher T 's. While it is easy to conjecture that the anomalies are due to the presence of 3d electrons of Cu (or 4d of Ag) in the valence bands, measurements of the dependence of the low temperature gap on isotopic mass would be desirable in order to tune these anomalies. Many of these chalcopyrites (e.g., Cu,Ga,Se) have three elements with more than one stable isotope each.

The present author was delighted to see, after completing this paper, a very recent article [94] in which the temperature renormalization of eight prominent structures, seen from 2 to 5 eV, in the reflectance anisotropy spectra of (100) InP surfaces were reported. The experimental data for the temperature shifts were fitted with single oscillators, i.e., with expressions similar

to Eq.(6). The zero-point renormalizations of most of the eight observed structures lie around -50 meV, rather similar to those of the bulk CP's. The fitted oscillator frequencies are close to the average phonon frequencies of bulk InP. As required by the oscillator fit, all observed frequencies depend linearly on T at high T . A square-root dependence is thus ruled out, at least for the frequency shifts.

References

- [1] A. Einstein, Ann. Physik **22**, 180 (1907).
- [2] W. Nernst and Lindemann, Preus. Akad. Wiss., Phys. Math. K., (1911), p. 494.
- [3] P. Debye, Ann. Physik **39**, 789 (1912).
- [4] E. Grüneisen, Handbuch der Physik **10**, 22 (1926).
- [5] J. Dong, O.F. Shankey, and C.W. Myles, Phys. Rev. Lett. **86**, 17 (2001).
- [6] A. Einstein, Ann. Physik **35**, 79 (1911).
- [7] K. Karch, T. Dietrich, W. Windl, P. Pavone, A.P. Mayer, and D. Strauch, Phys. Rev. B **53**, 7259 (1996).
- [8] H.Y. Fan, Phys. Rev. **82**, 900 (1951).
- [9] P.B. Allen and M. Cardona, Phys. Rev. B **27**, 4760 (1983); M.L. Cohen and D.J. Chadi, in “Handbook of Semiconductors”, Vol. II, M. Balkanski, editor, (North Holland, Amsterdam, 150) p. 155.
- [10] A. Debernardi, Solid State Commun. **113**, 1 (2000).
- [11] D. King-Smith, R.J. Needs, V. Heine, and M.J. Hodgson, Europhys. Lett. **10**, 569 (1989).
- [12] M. Rohlfing and S.G. Louie, Phys. Rev. Lett. **81**, 2312 (1998).
- [13] L.X. Benedict, E.L. Shirley, and R.B. Bohm, Phys. Rev. Lett. **80**, 4514 (1998).
- [14] S. Albrecht, L. Reining, R. del Sole, and G. Onida, Phys. Rev. Lett. **80**, 4510 (1998).
- [15] J.D. Brust, J.C. Phillips, and F. Bassani, Phys. Rev. Lett. **9**, 95 (1962).
- [16] M.L. Cohen and J. Chelikowsky, Electronic Structure and Optical Properties of Semiconductors, Springer, Heidelberg, 1989.
- [17] P. Etchegoin, J. Kircher, and M. Cardona, Phys. Rev. B **47**, 10292 (1993); *ibid* Phys. Rev. B **46**, 15139 (1992).
- [18] D. Rönnow, L.F. Lastras-Martínez, M. Cardona, and P.V. Santos, J. Opt. Soc. Am. A **16**, 568 (1999).
- [19] A. Lastras-Martínez, R.E. Banderas-Navarro, and L.F. Lastras-Martínez, Thin Solid Films **373**, 207 (2000).
- [20] C. Alibert, A.M. Joullie, A. Joullie, and R. Ranvaud, Nuovo Cimento **39**, 427 (1977).
- [21] M. Cardona, M.H. Grimsditch, D. Olego in Light Scattering in Solids, J.L. Birman and H.Z. Cummins (Eds.), Plenum Publ. Co., New York (1979), p. 249.
- [22] P. Etchegoin, J. Kircher, M. Cardona, and C. Grein, Phys. Rev. B **45**, 11721 (1992).
- [23] G. Theodorou, phys. stat. sol. b **211**, 847 (1999); *ibid* **211**, 29 (1999).

- [24] J.L.R. Hughes and J.E. Sipe, Phys. Rev. B **53**, 10751 (1998).
- [25] M. Cardona, L.F. Lastras-Martínez, and D.E. Aspnes, Phys. Rev. Lett. **83**, 3970 (1999).
- [26] L.F. Lastras-Martínez, T. Ruf, M. Konuma, M. Cardona, and D.E. Aspnes, Phys. Rev. B **61**, 12946 (2000).
- [27] A.T. Collins, S.C. Lawson, G. Davies, and H. Kanda, Phys. Rev. Lett. **65**, 891 (1960).
- [28] P. Etchegoin, J. Weber, M. Cardona, W.L. Hansen, K. Itoh, and E.E. Haller, Solid State Commun. **83**, 843 (1992).
- [29] P.B. Allen, Phil. Mag. **B70**, 527 (1994).
- [30] E. Antončík, Czech. J. Phys. **5**, 449 (1955).
- [31] F. Ciccacci, S. Selci, G. Chiarotti, and P. Chiaradia, Phys. Rev. Lett. **56**, 2411 (1986).
- [32] P. Pavone and S. Baroni, Solid State Commun. **90**, 295 (1994).
- [33] A. Debernardi and M. Cardona, Phys. Rev. B **54**, 11305 (1996).
- [34] H. London, Z. Phys. Chem. **16**, 302 (1958).
- [35] R.C. Buschert, A.E. Merlini, S. Pace, S. Rodríguez, and M.H. Grimsditsch, Phys. Rev. B **38**, 5219 (1988).
- [36] E. Sozontov, L.X. Cao, A. Kazimirov, V. Kohn, M. Konuma, M. Cardona, and J. Zegenhagen, Phys. Rev. Lett. **86**, 5329 (2001).
- [37] R.R. Reeber and K. Wang, J. Electronic Materials **25**, 63 (1996).
- [38] B.A. Weinstein and R. Zallen, in “Light Scattering in Solids IV”, M. Cardona and G. Güntherodt, editors, (Springer, Heidelberg, 1984) p. 463.
- [39] J. Serrano, unpublished.
- [40] K.G. Lyon, G.L. Salinger, C.A. Swenson, and K.G. White, J. Appl. Phys. **48**, 865 (1977).
- [41] P.B. Allen, Phys. Rev. B **18**, 5217 (1978).
- [42] D. Karaiskaj, M.L.W. Thewalt, T. Ruf, M. Cardona, H.J. Pohl, G.G. Deviatych, P.G. Sennikov, and H. Riemann, Phys. Rev. Lett. **86**, 6010 (2001).
- [43] M. Quintero, C. Rincon, R. Tovar, and J.C. Woolley, J. Phys. Condens. Matter **4**, 1281 (1992).
- [44] S. Zollner, M. Cardona, and S. Gopalan, Phys. Rev. B **45**, 3376 (1992).
- [45] P.Y. Yu and M. Cardona, Phys. Rev. B **2**, 3193 (1998).
- [46] P. Lautenschlager, P.B. Allen, and M. Cardona, Phys. Rev. B **31**, 2163 (1985).
- [47] C.D. Thurmond, J. Electrochem. Soc. **122**, 1133 (1975).

- [48] C. Parks, A.K. Ramdas, S. Rodríguez, K.M. Itoh, and E.E. Haller, Phys. Rev. B **49**, 14244 (1994).
- [49] The temperature dependence of a_0 for silicon and a fit similar to that of Fig. 3 will be found in: M. Cardona, Festschrift in honor of F. Bassani (Scuola Normale Superiore, Pisa, 2001).
- [50] H. Holloway, K.C. Hass, M.A. Tamar, T.R. Anthony, and W.F. Banholzer, Phys. Rev. B **44**, 7123 (1991).
- [51] A. Göbel, T. Ruf, M. Cardona, C.T. Lin, J. Wrzesinski, M. Steube, K. Reimann, J.-C. Merle, and M. Joucla, Phys. Rev. B **57**, 15183 (1998).
- [52] N. Garro, A. Cantarero, M. Cardona, A. Göbel, T. Ruf, and K. Eberl, Phys. Rev. B **54**, 4732 (1996).
- [53] Y.P. Varshni, Physica **34**, 149 (1967).
- [54] L. Viña, S. Logothetidis, and M. Cardona, Phys. Rev. B **30**, 1979 (1984).
- [55] A. Manoogian and A. Leclerc, Can. J. Phys. **57**, 1766 (1979).
- [56] R. Pässler, Solid State Electr. **39**, 1311 (1996).
- [57] A.T. Collins S.C. Lawson, G. Davies, and H. Kanda, Phys. Rev. Lett. **65**, 891 (1990).
- [58] M. Cardona and N.E. Christensen, Solid State Commun. **58**, 421 (1986).
- [59] R. Pässler, phys. stat. sol.(b), **200**, 155 (1997).
- [60] A. Göbel, T. Ruf, J.M. Zhang, R. Lauck, and M. Cardona, Phys. Rev. B **59**, 2749 (1999).
- [61] A. Zunger and M.L. Cohen, Phys. Rev. B **18**, 5449 (1978); *ibid* **20**, 4082 (1979).
- [62] M.T. Yin and M.L. Cohen, Solid State Commun. **43**, 391 (1982).
- [63] M.T. Yin and M.L. Cohen, Phys. Rev. B **26**, 3259 (1982).
- [64] R.W. Godby, M. Schlüter, and L.J Sham, Phys. Rev. Lett. **56**, 2415 (1986).
- [65] M. Cardona, Phys. Rev. **129**, 69 (1963).
- [66] J. Serrano and C. Schweitzer, unpublished results.
- [67] P. Lautenschlager, M. Garriga, S. Logothetidis, and M. Cardona, Phys. Rev. B **35**, 9174 (1987).
- [68] P.Y. Yu and M. Cardona, “Fundamentals of Semiconductors”, (Springer, Heidelberg, 2001, 3rd edition), p. 320.
- [69] P. Lawaetz, Thesis, The Technical University of Denmark, Lyngby, 1978 (unpublished).
- [70] D.E. Aspnes and A.A. Studna, Phys. Rev. B **7**, 4605 (1973).
- [71] D. Rönnow, L.F. Lastras-Martínez, and M. Cardona, Eur. Phys. J. **B5**, 29 (1998).

- [72] D.E. Aspnes and H. Arwin, *J.O.S.A.* **73**, 1759 (1983).
- [73] P. Lautenschlager, M. Garriga, L. Viña, and M. Cardona, *Phys. Rev. B* **36**, 4821 (1987).
- [74] P. Lautenschlager, P.B. Allen, M. Cardona, *Phys. Rev. B* **33**, 5501 (1986).
- [75] M. Cardona, L.F. Lastras-Martínez, and D.E. Aspnes, *Phys. Rev. Lett.* **83**, 3970 (1999); S. Albrecht, L. Reining, G. Onida, V. Olevano, and R. DelSole, *Phys. Rev. Lett.* **83**, 1971 (1999).
- [76] S. Selci, P. Chiaradia, F. Ciccacci, A. Cricenti, N. Sparvieri, and G. Chiarotti, *Phys. Rev. Lett.* **31**, 4096 (1985).
- [77] M.J. Olmstead and N.M. Amer, *Phys. Rev. B* **33**, 2564 (1986).
- [78] N.J. DiNardo, J.E. Demuth, W.A. Thompson, and P. Avouris, *Phys. Rev. B* **31**, 4077 (1985).
- [79] M.J. Olmstead and D.J. Chadi, *Phys. Rev. B* **33**, 8402 (1986).
- [80] C.D. Chen, A. Selloni, and E. Tosatti, *Phys. Rev. B* **30**, 7067 (1984).
- [81] R.K. Wehner and R. Klein, *Physica* **62**, 161 (1972).
- [82] T. Ruf, M. Cardona, C.S.J. Pickles, and R. Sussmann, *Phys. Rev. B* **62**, 16578 (2000).
- [83] F. Widulle, T. Ruf, M. Konuma, I. Silier, W. Kriegseis, V.I. Ozhogin, and M. Cardona, *Solid State Commun.* **118**, 1 (2001).
- [84] F. Widulle, J. Serrano, and M. Cardona, submitted to *Phys. Rev. B*.
- [85] J. Menéndez and M. Cardona, *Phys. Rev. B* **29**, 2051 (1984).
- [86] A. Debernardi, S. Baroni, and E. Molinari, *Phys. Rev. Lett.* **75**, 1819 (1995).
- [87] H.J. McSkimin and P. Andreatch, *J. Appl. Phys.* **43**, 2944 (1972).
- [88] H.J. McSkimin, *J. Appl. Phys.* **24**, 988 (1988).
- [89] A.K. Ramdas, S. Rodríguez, M. Grimsditch, T.R. Anthony, and W.F. Banholzer, *Phys. Rev. Lett.* **71**, 189 (1993).
- [90] R. Vogelgesang, A.K. Ramdas, S. Rodríguez, M. Grimsditch, and T.R. Anthony, *Phys. Rev. B* **54**, 3989 (1996).
- [91] M. Quintero, C. Rincon, R. Tovar, and J.C. Woolley, *J. Phys. Cond. Mat.* **4**, 1281 (1992).
- [92] V.A. Aliyev, G.D. Guseinov, F.I. Mamedov, and L.M. Chapanova, *Solid State Commun.* **59**, 745 (1986).
- [93] I.H. Choi and P.Y. Yu, *Phys. Rev. B* **63**, 235210 (2001).
- [94] S. Visbeck, T. Hannappel, M. Zorn, J.-T. Zettler, and F. Willig, *Phys. Rev. B* **63**, 245303 (2001).

| | $\Delta E(T = 0)$ | | dE/dM | | $\Delta E_{th}(T = 0)$ | dE_{th}/dM |
|------------------|-------------------|------|----------------|--------------|------------------------|--------------|
| Ge(E_g) | -53 | -53 | 0.36 | 0.37 | -13 | 0.09 |
| Ge(E_0) | -60 | -71 | 0.49 | 0.41 | -34 | 0.24 |
| Si(E_g) | -64 | -50 | 0.86 | 1.10 | +8 | -0.14 |
| diamond(E_g) | -615 | -340 | 13.6 | 17.1 | -88 | 3.6 |
| GaAs(E_0) | -90 | -110 | 0.39 | 0.32 | -38 | 0.16 0.11 |
| GaP(E_g) | -120 | | | | +5.3 | |
| ZnSe(E_0) | -65 | -64 | 0.22 0.22 | 0.19 0.26 | -15 | 0.12 0.04 |
| CuCl(E_0) | +30 | | -0.08 +0.36 | | -2.8 | |
| CuBr(E_0) | +6 | | -0.11 +0.12 | | -1.4 | |
| CuI(E_0) | +5 | | -0.55 - | | -3.5 | |

Table I: Zero-point anharmonic renormalization $\Delta E(T = 0)$ of the lowest gaps of several zincblende-type semiconductors (in meV) together with its derivative with respect to the isotopic mass (in meV/amu). Direct and indirect gaps are labeled E_0 and E_g , respectively. For completeness, the thermal expansion contribution to the zero-point parameters is also listed (ΔE_{th} and dE_{th}/dM). For the binary compounds the derivatives with respect to cation (above) and anion (below) masses are given. The first number under $\Delta E(T = 0)$ has been measured through linear extrapolation, except for diamond where a value calculated in [44] is given. The first number under dE/dM has been measured through isotopic substitution. The second numbers under ΔE and dE/dM were estimated from the measured values of dE/dM and ΔE , respectively, using Eq.(8). For sources see text.

| | dE_1/dM | $d(E_1 + \Delta_1)/dM$ | $\Delta E_1(T = 0)$ | $\Delta(E_1\Delta_1)(T = 0)$ |
|----|-------------------|------------------------|---------------------|------------------------------|
| Ge | 0.9 | 1.2 | 131 | 175 |
| | 0.45 ^a | | 65 ^a | |
| Si | 2.0 | – | 118 | – |
| | 1.2 ^a | | 71 ^a | |

^acalculated [44,46]

Table II: Derivatives of the E_1 and $E_1 + \Delta_1$ critical point energies of germanium at low temperatures as obtained from Figs. (9) and (10). Also, corresponding zero-point gap renormalizations estimated from the above values with Eq.(8) (in meV/amu and meV) and corresponding values for the E_1 critical point of silicon [26]. The experimental values measured by isotopic substitution are nearly a factor of two larger than those calculated using empirical pseudopotentials [44,46].